Journal Pre-proof

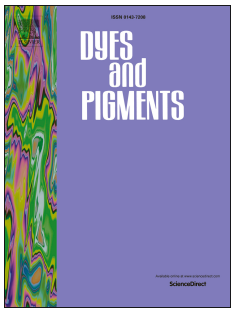

Near-infrared dual-functional AIEgens for lipid droplets imaging in multispecies and photodynamic therapy

Zhanguo Sun, Yaoming Liu, Pengli Guan, Binsheng Yang, Bin Liu

PII: S0143-7208(20)31581-3

DOI: https://doi.org/10.1016/j.dyepig.2020.108884

Reference: DYPI 108884

To appear in: *Dyes and Pigments*

Received Date: 4 June 2020

Revised Date: 13 August 2020

Accepted Date: 21 September 2020

Please cite this article as: Sun Z, Liu Y, Guan P, Yang B, Liu B, Near-infrared dual-functional AIEgens for lipid droplets imaging in multispecies and photodynamic therapy, *Dyes and Pigments*, https://doi.org/10.1016/j.dyepig.2020.108884.

Zhanguo Sun: Investigation, Designed, Synthesis, Writing original draft. **Yaoming Liu:** Biological and imaging experiments. **Pengli Guan:** Date analysis. **Binsheng Yang:** Supervision, Writing-review and editing. **Bin Liu:** Supervision, Date analysis, Funding acquisition.

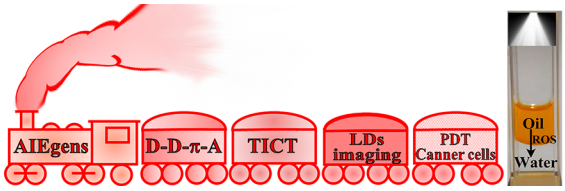

Near-infrared dual-functional AIEgens for lipid droplets imaging in multispecies and photodynamic therapy

Zhanguo Sun[a,b], Yaoming Liu[c], Pengli Guan[a], Binsheng Yang[a]*, Bin Liu[a]*

[a] *Key Laboratory of Chemical Biology and Molecular Engineering, Ministry of Education, Institute of Molecular Science, Shanxi University, Taiyuan, 030006, China*

[b] *Institute of Carbon Materials Science, Shanxi DaTong University, DaTong, Shanxi province, 037009, China*

[c] *Scientific Instrument Center of Shanxi University, Taiyuan, China*

ABSTRACT

Lipid droplets (LDs) are important organelles with hydrophobic structure that not only served the function of lipid storage in cells but also participate in the regulation of numerous metabolic processes. Broad visualization of LDs with high brightness is important for biological applications. In this study, three novel facile near-infrared aggregation-induced emission (AIE) fluorescent bioprobes based on triphenylamine-pyridine building block were designed and synthesized. These AIEgens block exhibits tunable D-D-π-A (D: donor, A： acceptor) structure with twisted intramolecular charge transfer (TICT) characteristics. These bioprobes can highly light up LDs in the living cells, model animal zebrafish and shelled sunflower seed. More importantly, these probes can effectively produce reactive oxygen species (ROS) in the presence of light irradiation, leading to the apoptosis of cancer cells. This study exhibits promising applications in photodynamic therapy through targeting LDs.

Keywords: Lipid droplets, Multispecies imaging, Aggregation-induced emission (AIE), Photodynamic therapy.

1. Introduction

Lipid droplets (LDs) are widespread neutral lipid-rich subcellular organelles in eukaryotic and prokaryotic cells. LDs are delimited by a single phospholipid monolayer and primarily contain triacylglycerol and cholesteryl esters [1]. For a long time after their discovery, LDs had been considered simple lipid storage depots. However, several studies have reported that LDs as a dynamic organelle can regulate many physiological processes, such as lipid metabolism and storage, membrane transfer, and signal transduction [2-4]. Abnormal lipid storage may be related to many diseases, such as obesity, fatty liver, cardiovascular disease, and diabetes [5-8]. Hence, specific locating and imaging of LDs in cells and other model organisms are important to biomedical research and early-stage diagnosis of related diseases.

In recent years, many technologies have been developed for imaging LDs, such as ^{1}H nuclear magnetic resonance (NMR) spectroscopy [9], raman scattering imaging [10], and ultrahigh-resolution grazing incidence-structured illumination microscopy imaging [11]. However, these methods have certain disadvantages, such as high application cost and complex operation process, which limit their wide application in biological research. By contrast, fluorescence imaging technology has the advantages of high sensitivity, non-invasiveness, low cost, and features a user-friendly control. In addition, this technology is becoming one of the widely used in biological analysis and detection [12,13]. Several types of conventional fluorescent dyes, such as Sudan III, BODIPY493/503, Nile Red, and decorative boron-dipyrromethene (BODIPY) dye LD540, were utilized to image LDs. Although these fluorophore dyes can target LDs, they often suffer from background noise and small Stokes shifts due to their structural defects. Moreover, the aggregation-caused quenching (ACQ) phenomenon results in poor photostability of the dyes, making them unsuitable for long-term staining observation of LDs in biological applications [14-17].

Aggregation-induced emission (AIE), which was originally proposed by Tang and colleagues in 2001, has been proved to be the opposite of the ACQ phenomenon [18]. Organic fluorescent compounds with AIE characteristics can satisfactorily solve the self-quenching phenomenon of traditional fluorophores in a high-concentration

solution. AIEgens are widely used in imaging applications because of their excellent optical stability, high signal-to-noise ratio, and large Stokes shift [19]. Moreover, certain AIEgens used as a photosensitizer can produce reactive oxygen species (ROS) under light irradiation to kill cancer cells and thus can be used in photodynamic therapy (PDT) [20].

Near-infrared (NIR) fluorescence imaging is urgently needed in high-quality bioimaging because of its outstanding advantages, such as its ability to eliminate background fluorescence interference and penetrate deep tissues [21,22]. Lengthening the π-conjugated structure or increasing the push–pull effect of molecules is an effective way to construct AIE fluorescent probes with NIR emission characteristics [23,24]. To date, various NIR AIEgens bridged with benzene, thiophene, or carbazole rings have been reported in LDs imaging [25,26]. However, their shortcomings, such as low conjugation or complex preparation process, must be improved. Previous studies have demonstrated that AIEgens with a strong push–pull structure can produce ROS when exposed to light [27,28]. This finding inspired us to design novel bridge-linked molecules with strong push–pull structure and has the character of NIR emission. These molecules can be used in NIR fluorescence bioimaging of multispecies and PDT study on cells.

Herein, three kinds of small molecule NIR red AIEgens (namely, TPAP-Ma, TPAP-Is, and TPAP-Fu) with strong push–pull effect of D-D-π-A structure were designed and synthesized. These probes are bridged with pyridine ring and connected by triphenylamine group as strong electron donor and three gradually enhanced strong electron acceptor group (namely, malononitrile, isophorone, and 3-cyano-4-phenyl-2(5H)-furanone). These probes show bright-red NIR emission, excellent optical properties, remarkable stability, and efficient ROS generation. As shown in Scheme 1, these AIEgens can highly imaging of LDs in common living cells，even in the model animal zebrafish and oil crop sunflower seeds. Moreover, they show potential applications for cancer cell ablation. We also preliminarily explored the distribution of ROS in oil phase and water phase by fluorescence spectra.

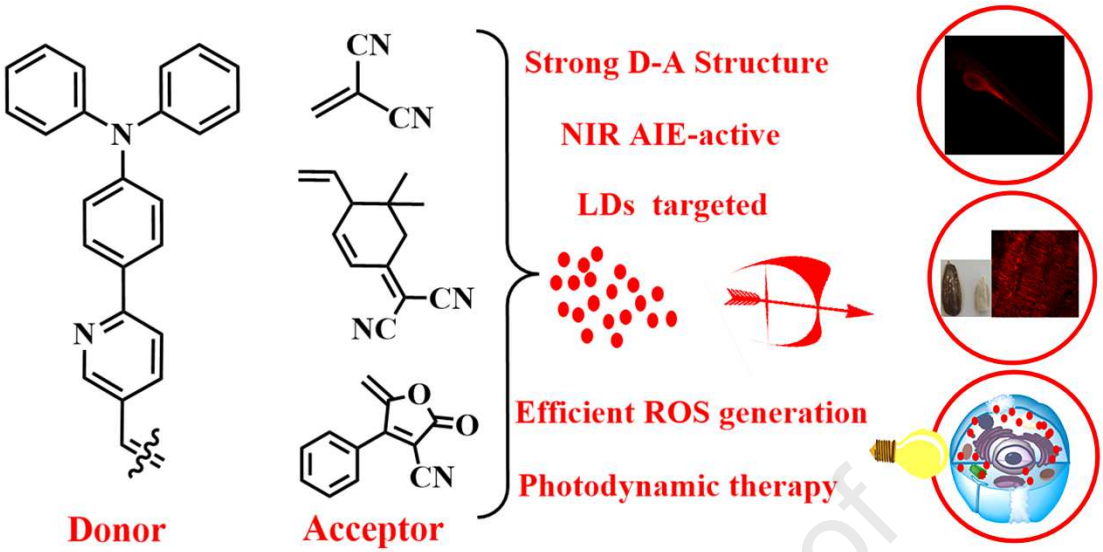

Scheme 1. The features and application diagram of AIEgens.

2. Experimental methods

2.1. Materials

All chemical reagents and analytical pure solvents were purchased from commercial companies without further purification prior to use. ^{1}H and ^{13}C NMR spectra were measured on a BRUKER AVANCE III 600 NMR using $CDCl_3$ as solvents and tetramethylsilane as an internal standard (Germany). High-resolution mass spectrometry (HRMS) electrospray ionization spectra were obtained using a Thermo Scientific Q Exactive (USA). UV-vis absorption spectra were measured on a VARIAN 50 Bio-spectrophotometer (USA). PL spectra were recorded using a VARIAN Eclipse spectrophotometer (USA). Absolute fluorescence quantum yields were measured on a FLS 980 spectrophotometer (UK). The images of cells and tissues were taken using a Zeiss LSM 880 laser scanning confocal microscope (Germany).

2.2. Synthesis process

The synthetic route of precursor TPAP-CHO, TPAP-Ma, TPAP-Is, and TPAP-Fu was shown in Scheme 2. TPAP-CHO was synthesized according to the previous literature [29]. ^{1}H NMR (600 MHz, $CDCl_3$, TMS), δ (ppm): 10.11 (s, 1H), 9.08 (s, 1H), 8.20 (d, *J* = 7.96 Hz, 1H), 8.00 (d, *J* = 8.58 Hz, 2H), 7.84 (d, *J* = 8.29 Hz, 1H), 7.34 (t, *J* = 7.70 Hz, 4H), 7.15-7.19 (m, 6H), 7.13 (t, *J* = 7.26 Hz, 2H).

Synthesis of compound TPAP-Ma. TPAP-CHO (350.5 mg, 1.0 mmol) and malononitrile (66.1 mg, 1.0 mmol) was dissolved in 20 mL anhydrous ethanol with a drop of piperidine refluxed for 4 h. After cooling to room temperature, the red solid was filtered, washed with ice-anhydrous ethanol, and dried to give a red power named TPAP-Ma (262.4 mg, 66%). ^{1}H NMR (600 MHz, $CDCl_3$, TMS), δ (ppm): 8.84 (s, 1H), 8.55 (d, *J* = 8.34 Hz, 1H), 8.01 (d, *J* = 8.39 Hz, 2H), 7.86 (d, *J* = 8.66 Hz, 1H), 7.77 (s, 1H)，7.36 (t, *J* = 7.56 Hz, 4H), 7.20 (d, *J* = 7.73 Hz,4H), 7.16 (t, *J* = 9.06 Hz, 4H). ^{13}C NMR (100 MHz, $CDCl_3$) δ (ppm): 161.45, 156.07, 153.37, 150.80, 146.71, 135.97, 129.58, 128.66, 125.67, 124.48, 124.36, 121.45, 119.47, 113.65, 112.74, 82.37. HRMS (ESI): $[M + H]^+$ for $C_{27}H_{18}N_4$ calcd: 399.16042, found 399.16046.

Synthesis of compound TPAP-Is. 2-(3,5,5-trimethylcyclohex-2-en-1-ylidene) malono-nitrile was synthesized according to the reported literature [30]. TPAP-CHO (350.2 mg, 1.0 mmol) and 2-(3,5,5-trimethylcyclohex-2-en-1-ylidene)malononitrile (186.4 mg, 1.0 mmol) was dissolved in 20 mL anhydrous ethanol with a drop of piperidine refluxed for 4 h. After cooling to room temperature, the red solid was filtered, washed with ice-anhydrous ethanol, and dried to give a red power named TPAP-Is (407.8 mg, 78%). ^{1}H NMR (600 MHz, $CDCl_3$, TMS), δ (ppm): 8.72 (s, 1H), 7.94 (t, *J* = 8.70 Hz, 3H), 7.74 (d, *J* = 8.40 Hz, 1H), 7.31 (t, *J* = 7.68 Hz, 4H), 7.17 (t, *J* = 7.07 Hz, 6H), 7.10 (t, *J* = 7.32 Hz, 3H), 7.07 (d, *J* = 2.27 Hz, 1H), 6.90 (s, 1H), 2.64 (s, 2H), 2.52 (s, 2H), 1.12(s, 6H). ^{13}C NMR (100 MHz, $CDCl_3$) δ (ppm): 169.07, 157.55, 153.21, 149.84, 149.35, 147.23, 133.68, 133.17, 129.93, 129.41, 129.06, 127.82, 125.05, 124.11, 123.62, 122.63, 119.71, 112.65, 79.27, 43.00, 39.16, 32.07, 28.05. HRMS (ESI): $[M + H]^+$ for $C_{36}H_{30}N_4$ calcd: 519.25432, found 519.25449.

Synthesis of compound TPAP-Fu. 2-oxo-4-phenyl-2,5-dihydrofuran-3-carbonitrile was synthesized according to the reported literature [31]. TPAP-CHO (350.2 mg, 1.0

mmol) and 2-oxo-4-phenyl-2,5-dihydrofuran-3-carbonitrile (185.5 mg, 1.0 mmol) was dissolved in 20 mL anhydrous ethanol with a drop of piperidine refluxed for 4 h. After cooling to room temperature, the red solid was filtered, washed with ice-anhydrous ethanol, and dried to give a red power named TPAP-Fu (360.7 mg, 69%). ^{1}H NMR (600 MHz, $CDCl_3$, TMS), δ (ppm): 8.79 (s, 1H), 8.45 (s, 1H), 7.98 (d, *J* = 6.60 Hz, 2H), 7.81 (d, *J* = 7.25 Hz, 1H), 7.69 (s, 5H), 7.32 (s, 4H), 7.12-7.19 (m, 8H), 6.51 (s, 1H). ^{13}C NMR (100 MHz, $CDCl_3$) δ (ppm):163.56, 158.17, 152.83, 149.94, 147.01, 146.79, 138.36, 132.58, 130.77, 129.77, 129.48, 128.98, 128.20, 127.36, 125.92, 125.31, 123.93, 122.13, 119.70, 117.56, 111.51, 99.38. HRMS (ESI): $[M + H]^+$ for $C_{35}H_{23}N_3O_2$ calcd: 518.18630, found 518.18608.

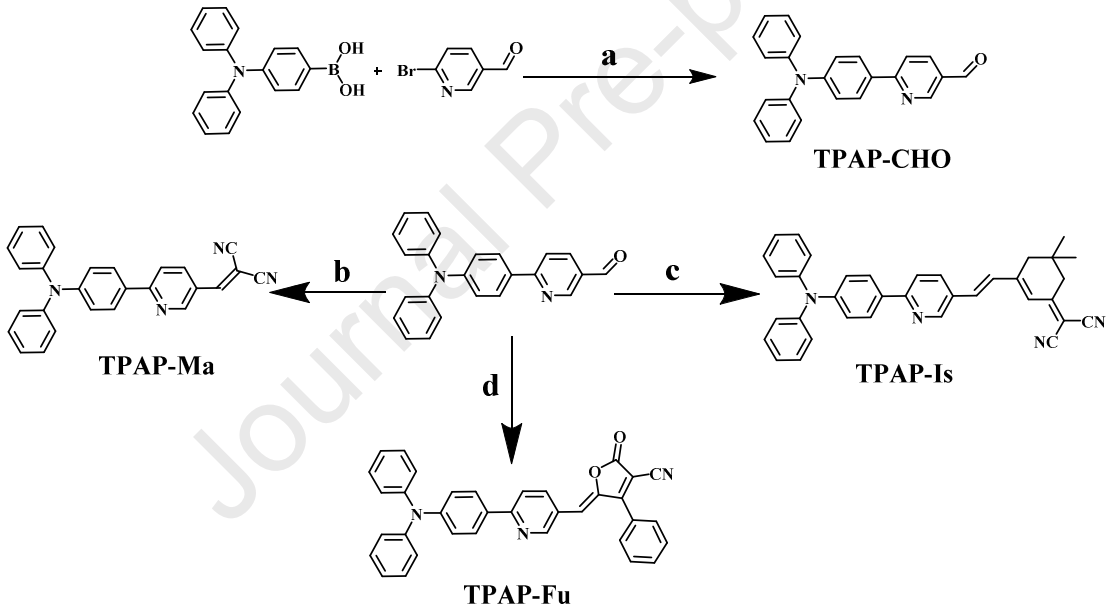

Scheme 2. Synthetic routes of three probes. Reagents and conditions: (a) $Pd(dppf)Cl_2$, K_2CO_3, Isopropyl alcohol; (b) malononitrile; (c) 2-(3,5,5-trimethylcyclohex-2-en-1-ylidene) malononitrile; (d) 2-oxo-4-phenyl-2,5-dihydrofuran-3-carbonitrile.

2.3. Cytotoxicity study

The cytotoxicity of three probes was investigated via 3-(4,5-dimethyl-2-thiazolyl)-2,5-diphenyltetrazolium bromide (MTT) assay. PC12 cells were cultured in a RPMI-1640 medium containing 10% heat-inactivated fetal bovine serum, penicillin (100

$U \cdot mL^{-1}$), and streptomycin (100 $\mu g \cdot mL^{-1}$) at 37 °C in a humidified 5% CO_2 incubator and passed down for 2-3 days once. The cell was seeded at a density of 5000 cells per well in a 96-well plate. After culturing overnight, various concentrations (0, 0.78, 1.56, 3.12, and 6.25 μM) of certain dyes (namely, TPAP-Ma, TPAP-Is, and TPAP-Fu) were added for 24 h. Subsequently, the medium was removed in each well and the cell was washed with phosphate-buffered saline (PBS), fresh medium (1.99 mL) and MTT (10 μL, 0.5 mg mL^{-1}) solution was added to each cell for 4 h. Afterward, all the medium was discarded and DMSO (2.0 mL) was added to each well. The plate was gently vibrated for a few minutes to dissolve all the formed precipitates. The absorption of the probes and control well at 570 nm was recorded using a microplate reader. SMMC-7721 cells were cultured in a similar manner, and MTT assay was performed.

2.4. Bioimaging of LDs in living cells and tissues

PC12 cells (rat pheochromocytoma cells), zebrafish, and sunflower seeds were selected as the models for bioimaging experiments. PC12 cells were grown in a 20 mm glass bottom cell culture dish with a coverslip at 37 °C. A recognized LDs target dye BODIPY493/503 green (1 μM) and each probe (1 μM) were added into different cell Petri dishes at 37 °C for 15 min. Four-day-old zebrafish incubated in E3 medium and sunflower seeds cut as thinly as possible with a blade were selected as subsequent experimental objects. Both models were dyed and co-incubated in a manner similar to the aforementioned conditions. Afterward, all the selected models were washed with PBS buffer three times, and the fluorescence images were observed under a confocal laser microscope with the following conditions: for the three probes and BODIPY493/503 green (λ_{ex} = 488 nm, λ_{em} = 600-700 nm and 500-550 nm), respectively.

2.5. Photostability

The PC12 cells labeled with synthesized dyes and BODIPY493/503 were imaged

using a Zeiss LSM 880 laser scanning confocal microscope. For all the three probes (TPAP-Ma, TPAP-Is, and TPAP-Fu) and BODIPY493/503 green, the excitation was set at 488 nm with 1% laser power irradiation intensity, and the emission filter was 600-700 nm and 500-550 nm, respectively. Continuous scans were performed at 22.4 s per scan.

2.6. ROS-generation detection

2,7-dichlorodihydrofluorescein diacetate (H2DCF-DA), a recognized ROS detection reagent, was used in the experiment. Frist, H2DCF-DA was activated into DCF-DA by sodium hydroxide solution. Then certain amount of probe solution was added to 1 mL of DCF-DA (40 μM) mixed evenly to prepare the final concentration of probes (5 μM). The fluorescence intensity of DCF-DA at 525 nm was recorded under white light (30 mW/cm^2) irradiation at various times.

2.7. Cytotoxicity of probes to SMMC-7721 cells under white light irradiation

SMMC-7721 cells were seeded at a density of 5000 cells per well in a 96-well plate. After culturing in RPMI-1640 medium overnight, the cells were treated with various concentrations of TPAP-Ma, TPAP-Is, and TPAP-Fu in fresh medium for 30 min. Subsequently, the plates containing SMMC-7721 cells were irradiated for 30 min at a white light source of 30 mW/cm^2, and another row of plates treated under the same conditions were placed in the dark as a control.

3. Results and discussion

3.1. Design and synthesis

It is well known that molecules with strong push-pull structure and high π-conjugated structure tend to form intramolecular charge-transfer (ICT) characteristics,

obvious red-shift emission, and ROS generation under irradiation [24,28]. In order to achieve the purpose, triphenylamine, a widely used electron donor group, was used to construct AIE molecules [32]. As depicted in Scheme 2, three novel AIEgens, denoted as TPAP-Ma, TPAP-Is, and TPAP-Fu, were synthesized through Knoevenagel condensation reaction in anhydrous ethanol solvent. Reaction of TPAP-CHO precursor and different progressively enhanced electron-withdrawing groups (malononitrile, isophorone, and 3-cyano-4-phenyl-2(5H)-furanone) was catalyzed by piperidine under anhydrous ethanol solvent. All the intermediates and three final compounds were purified by flash column chromatography or recrystallization, with good yields ranging from 63% to 86%, and the structure were characterized by ^{1}H NMR, ^{13}C NMR, and HRMS (Fig. S1-S11).

3.2. Photophysical properties

The optical properties of TPAP-Ma, TPAP-Is, and TPAP-Fu were determined by UV-vis and photoluminescence spectrum. The maximum absorption spectrum of TPAP-Ma, TPAP-Is, and TPAP-Fu in toluene peaked at 472, 477, and 508 nm, respectively (Fig. 1A). From the view of molecular structure, although TPAP-Is and TPAP-Ma has almost the same electron-withdrawing group malononitrile and triphenylamine electron donor groups, TPAP-Is has a longer π-conjugated than TPAP-Ma, which result in a redshift emission of TPAP-Is. In addition, TPAP-Fu has the largest absorption peak due to its long π-conjugated structure and the strongest electron-withdrawing group (malononitrile < isophorone < 3-cyano-4-phenyl-2(5H)-furanone) [26]. This is consistent with the reported literature that NIR emission fluorescence molecules can be constructed by enhancing the ICT effect of molecules and prolonging π-conjugated structures [24].

In addition, the compounds presented good solubility in organic solvents with successively enhanced polarity, such as toluene, dioxane, ethyl acetate, tetrahydrofuran, and dichloromethane. As shown in Fig. 1B, S12, the solvent produced a weak effect on the absorption spectrum of all compounds, whereas a

remarkable positive solvent effect was observed on the fluorescence spectrum as shown in Fig. 1C, S13. The maximum emission of representative TPAP-Is had a large red shift (λ_{em}) from 615 nm to 741 nm with increasingly enhanced polarity from toluene to dichloromethane. Considering that all these compounds emitted in the red/near-infrared region, the quantum yields Φ_l (%) are an important indicator to test the practical use for the NIR florescent probes. As shown in Fig.S14, the Φ_l (%) of TPAP-Ma, TPAP-Is and TPAP-Fu are 81.98, 52.27, 48.36 in toluene (a lower polarity solvent), which are pretty high for D-D-π-A molecules. So, such probes can light up low-polarity organelle in cells, laying the foundation for its LDs recognition. In addition, the Φ_l (%) of TPAP-Is are 50.99, 1.48, 1.06, 1.09 in other solvent with increased polarity from dioxane to dichloromethane. Meanwhile, the fluorescence intensity was considerably reduced or even quenched in the strong polar solvent acetone and dimethyl sulfoxide (DMSO), suggesting a strong twisted intramolecular charge transfer (TICT) effect [33].

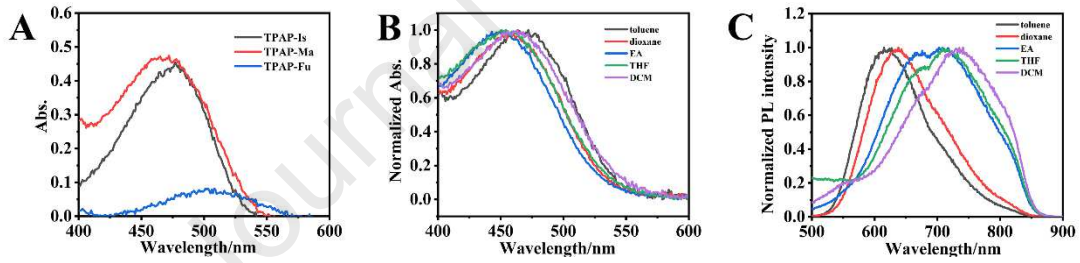

Fig. 1. (A) Absorption spectra of TPAP-Ma, TPAP-Is, and TPAP-Fu (10 μM) in pure toluene. (B) Normalized absorption spectra of representative TPAP-Is in different polar solvents. (C) normalized PL spectra of representative TPAP-Is in different polar solvents.

The AIE property of TPAP-Ma, TPAP-Is, and TPAP-Fu was investigated in DMSO/water mixtures with different water fractions (f_w) (Fig. 2A and S15). In pure DMSO solutions, all three probes showed weak red emission. Gradually increasing f_w from 0 to 50 (for TPAP-Ma) or 20 vol% (for TPAP-Is and TPAP-Fu) resulted in a slow quenching in fluorescence intensity due to the intrinsic TICT effect of a strong dipole compound. As f_w continued to increase, fluorescence intensity of the

compounds greatly increased. This result is attributed to the fact that the effect of aggregating effect exceeded the TICT effect, thereby limiting the free rotation of the molecule and leading to a decrease in non-radiative transition and an increase in radiative transition [34]. When f_w reached 80% (for TPAP-Ma and TPAP-Fu) or 60% (for TPAP-Is), the compounds showed the strongest fluorescence intensity. The Φ_l (%) of TPAP-Is in DMSO/H_2O (f_w = 60%) is 2.15 with NIR emissions at 675 nm, which is not lower compared with the reported NIR LDs probes (Table S1). In addition, their emission intensities were boosted by 9- , 27- , and 10-fold (Fig. 2B). As f_w continued to increase, further aggregation of the molecules led to a sharp decrease in fluorescence intensity. These results indicate that TPAP-Ma, TPAP-Fu, and TPAP-Is are AIE molecules in the NIR region with a maximum emission peak at 653, 675, and 745 nm, respectively.

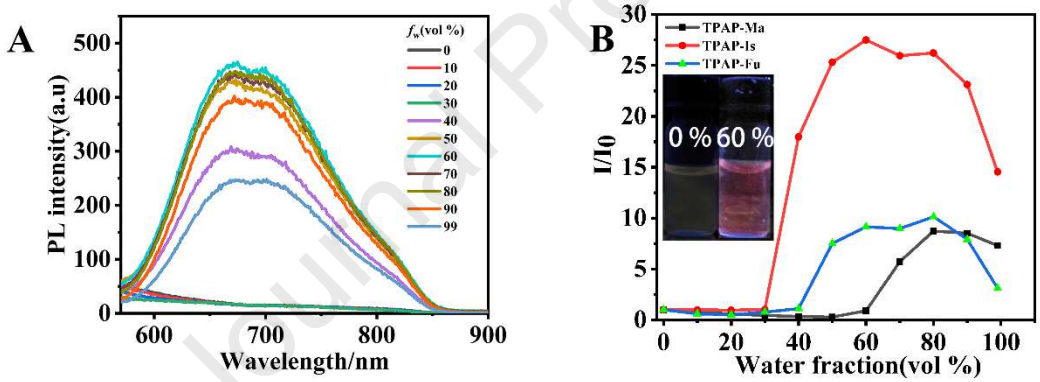

Fig. 2. (A) PL spectra of TPAP-Is (10 μM) in DMSO/water mixtures with different water fractions (f_w). (B) Plot of relative PL intensity (I/I_0) of all the synthesized compounds (10 μM) with different water fractions (f_w) in DMSO/water mixtures. Inset: fluorescent image of TPAP-Is (10 μM) in DMSO solution and in DMSO/water mixtures with f_w = 60% taken under 365 nm light.

3.3. Theoretical calculations

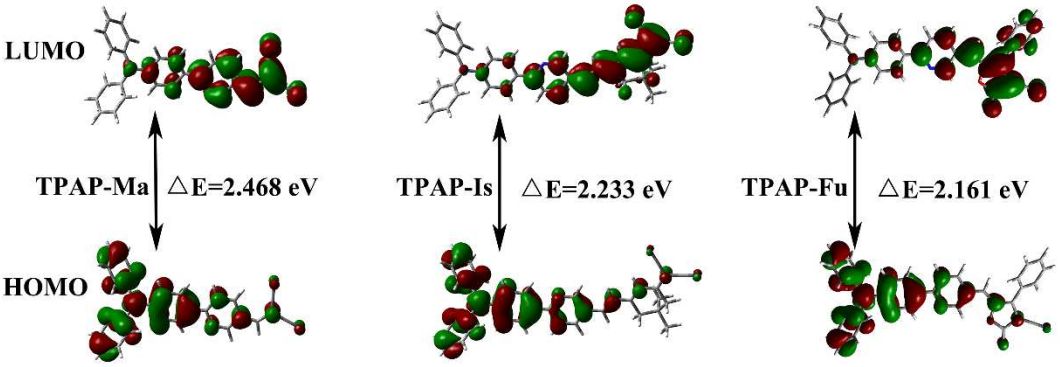

Fig. 3. Molecular orbital amplitude plots of HOMO and LUMO of TPAP-Ma, TPAP-Is, and TPAP-Fu calculated at the B3LYP/6-31G (d, p) level.

To further understand the optical characteristics of these fluorophores, we applied density functional theory to analyze the band gap of the three fluorophore groups. As presented in Fig. 3, the electron cloud density of the HOMO orbital is primarily distributed on the triphenylamine group and the pyridine ring in the center, whereas the LUMO energy level is mainly distributed on various electron-withdrawing groups. The calculation results revealed that these AIEgens (TPAP-Ma, TPAP-Is, and TPAP-Fu) had the same electron-donating group TPA and bridged pyridine ring. The stronger the electron-withdrawing group is, the smaller the energy band gap will be. This trend is in good accordance with the UV-vis spectral data and satisfactorily illustrated the progressively enhanced ICT effect. Moreover, the intersystem crossing can occur more readily than the usual molecules, which is attributed to the TICT characteristics of these AIEgens [35]. The singlet-triplet energy gaps (ΔE_{S1-T1}) of TPAP-Ma, TPAP-Is, and TPAP-Fu was calculated 0.5607, 0.6256 and 0.4913 eV by time-dependent density functional theory (Fig S16). As being demonstrated in literatures, D-D-π-A structure of AIEgens has narrow band gap, which prompted effective separation of HOMO and LUMO distribution and result in smaller ΔES1-T1. It will be beneficial to the production of ROS under light irradiation [36,37]. These results provided potential application value for the synthesized compounds in the field of photodynamic therapy.

3.4. Bioimaging in living cells

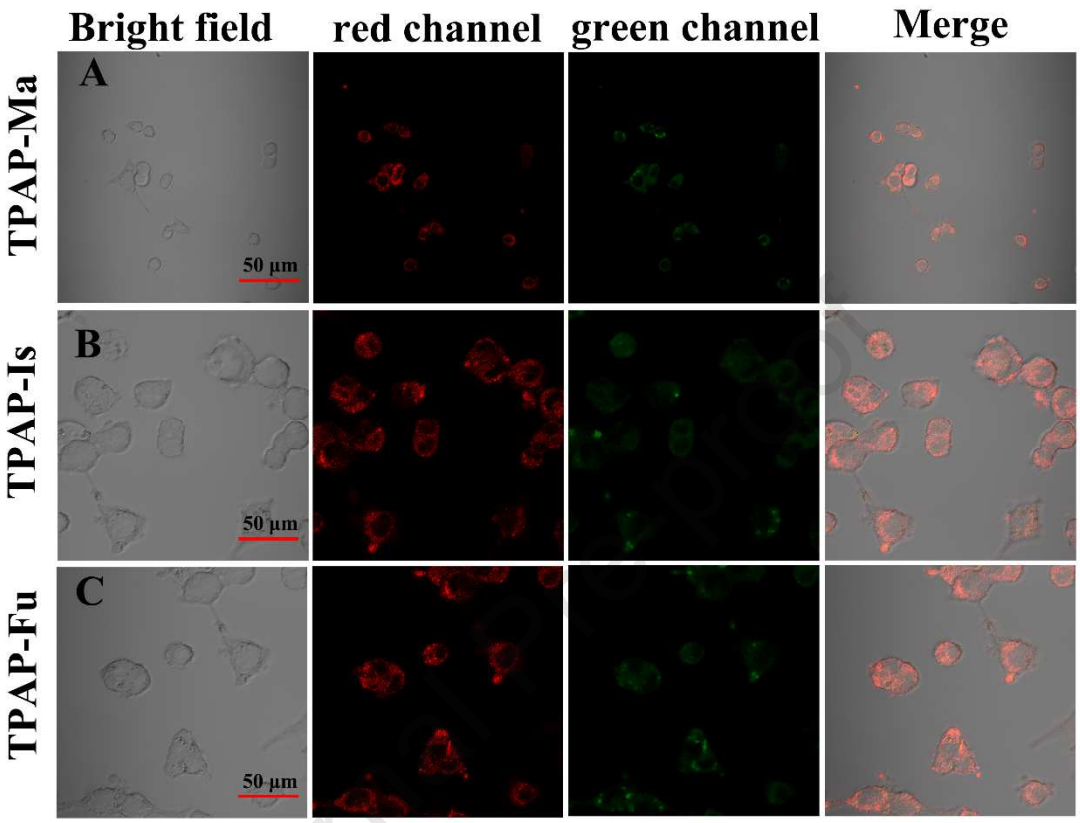

Fig. 4. Co-localization imaging of PC12 cells stained with BODIPY 493/503 and AIEgens: (A) TPAP-Ma, (B) TPAP-Is, (C) TPAP-Fu. λex = 488 nm. Concentration: 1 μM (BODIPY 493/503 and AIEgens). Scale bar: 50 μm.

As one of the key conditions of fluorescent dyes in cell imaging experiments, the presented AIE fluorophores need low dark toxicity to ensure good biocompatibility. PC12 cells were selected as a model to analyze the dark toxicity of TPAP-Ma, TPAP-Is, and TPAP-Fu via MTT assay. As shown in Fig. S17, cell viability was nearly 100% when the concentration of probe increased to 6.5 μM, demonstrating the negligible toxicity and good biocompatibilities of these AIEgens to living PC12 cells.

Photostability is another important criterion for evaluating these AIE fluorophores. PC12 cells stained with fluorescent dyes were continuously scanned under a laser confocal microscope to quantitatively measure the photostability of the dyes. As

shown in Fig. S18, the fluorescent intensity of the traditional commercial LDs dye, BODIPY 493/503 Green, was reduced to 54% of the initial intensity after a continuous scan of 40 scans within 10 min. By contrast, the loss in fluorescence intensity of TPAP-Ma was negligible. Moreover, TPAP-Is and TPAP-Fu were slightly reduced to 87% and 85%, respectively. The results showed that these three AIEgens have better photostability than the commercial LDs probe BODIPY 493/503 Green.

The three probes exhibited excellent photostability and low dark toxicity. In addition, the logarithm of octanol-water partition coefficient (Log *P*) was 6.43, 8.53, and 7.03 for TPAP-Ma, TPAP-Is, and TPAP-Fu estimated from ChemBioDraw software, respectively. As an important measure of the ability of neutral LD probe molecules, molecules with Log $P > 5.00$ can easily target LDs through the lipid membrane [38]. These results prompted us to investigate the ability of the probes to image endogenous LDs in living cells.

BODIPY 493/503 Green, an approved commercial green LD-targeting dye, was selected as one of the standard reagents to evaluate the ability of the three synthesized probes to target LDs. PC12 cells were incubated with BODIPY 493/503 Green (1 μM) and each AIEgen fluorophore (1 μM) for 15 min. As shown in Fig. 4, in contrast to the background observed under bright field, the bright red of each probe and green fluorescence of BODIPY 493/503-stained PC12 cells can be clearly observed from the red and green channels. The merging of PC12 cell images overlapped well, demonstrating that these AIE fluorophores have a highly ability to target LDs. Moreover, these AIE fluorophores have good lipophilicity and permeability to the cell membrane; therefore, these AIE fluorophores was more inclined to aggregated in hydrophobic spherical LDs and targeted staining with the aid of “like-like” interactions. In addition, since the environmental polarity of cytoplasm is higher than that of LDs, the trace amounts of the probe molecule hardly emits fluorescence in cytoplasm due to the TICT properties of the probe.

3.5. Zebrafish imaging

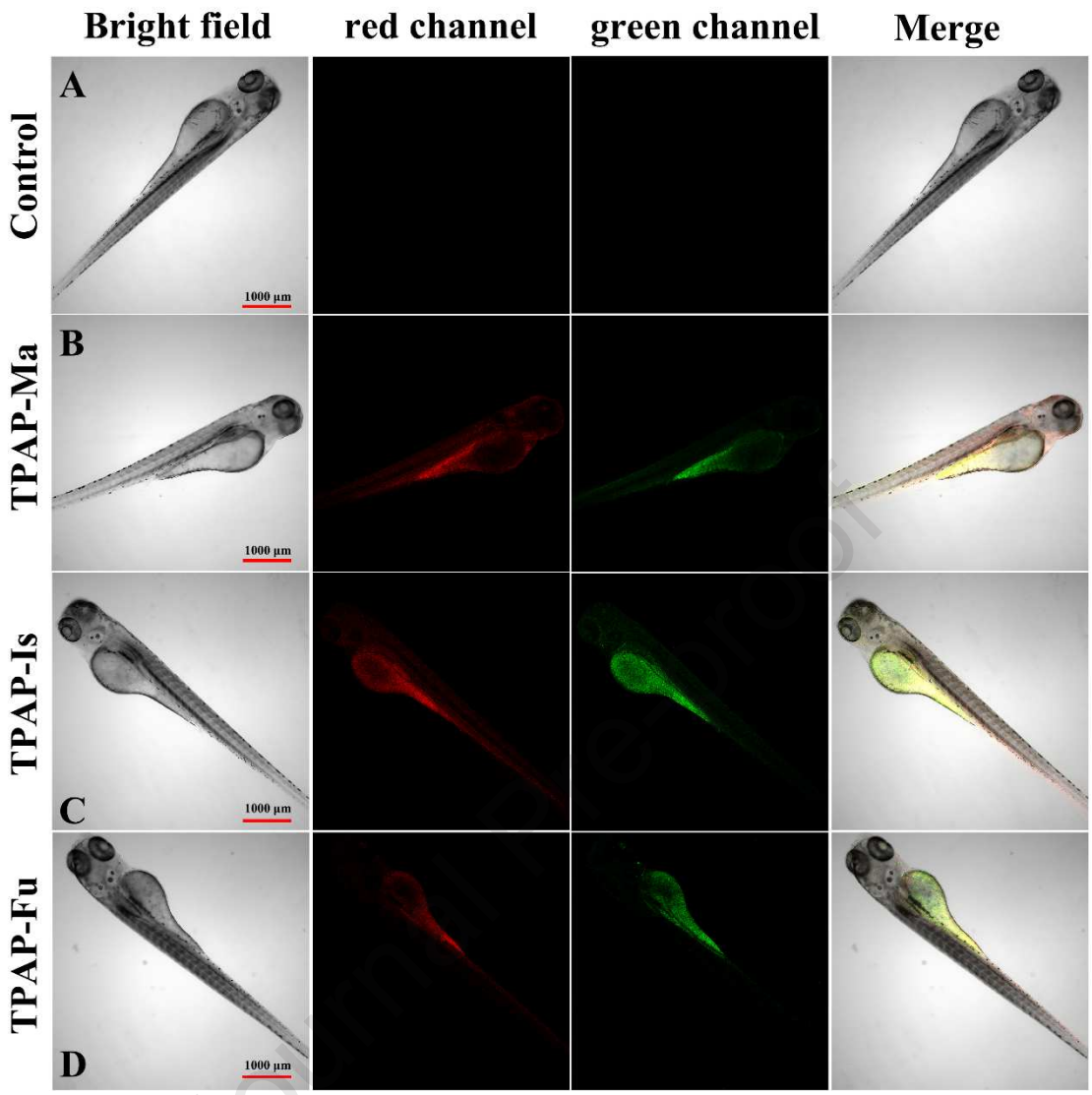

Fig. 5. (A) Untreated zebrafish served as a control. Co-localization imaging of zebrafish stained with BODIPY 493/503 and AIEgens: (B) TPAP-Ma, (C) TPAP-Is, (D) TPAP-Fu. λex = 488 nm. Concentration: 1 μM (BODIPY 493/503 and AIEgens). Scale bar: 1000 μm.

Zebrafish, which is often used as a model organism for in vivo biological imaging experiments, is one of the most important model vertebrates in the life sciences because of its high homology with human genes [39]. Owing to the red fluorescence emission and remarkable target LD-staining ability of AIE fluorophores in living PC12 cells, their potential application in imaging LDs in zebrafish was explored. As shown in Fig. 5, the 4-day-old zebrafish in E3 medium was eluted with PBS as a control. Almost no fluorescence was observed in each channel under the laser

confocal microscope. After co-pre-incubation with TPAP-Ma, TPAP-Is, TPAP-Fu (1 μM), and BODIPY 493/503 Green (1 μM), bright red and green co-dye-stained zebrafish was observed in the corresponding channel. The merged image shows better coincidence degree for the probes TPAP-Ma and TPAP-Is. Moreover, the overlap coefficient is 0.85 and 0.84 (Fig. S19). These results demonstrate that the probes can image endogenous LDs in zebrafish.

3.6. Sunflower seed imaging

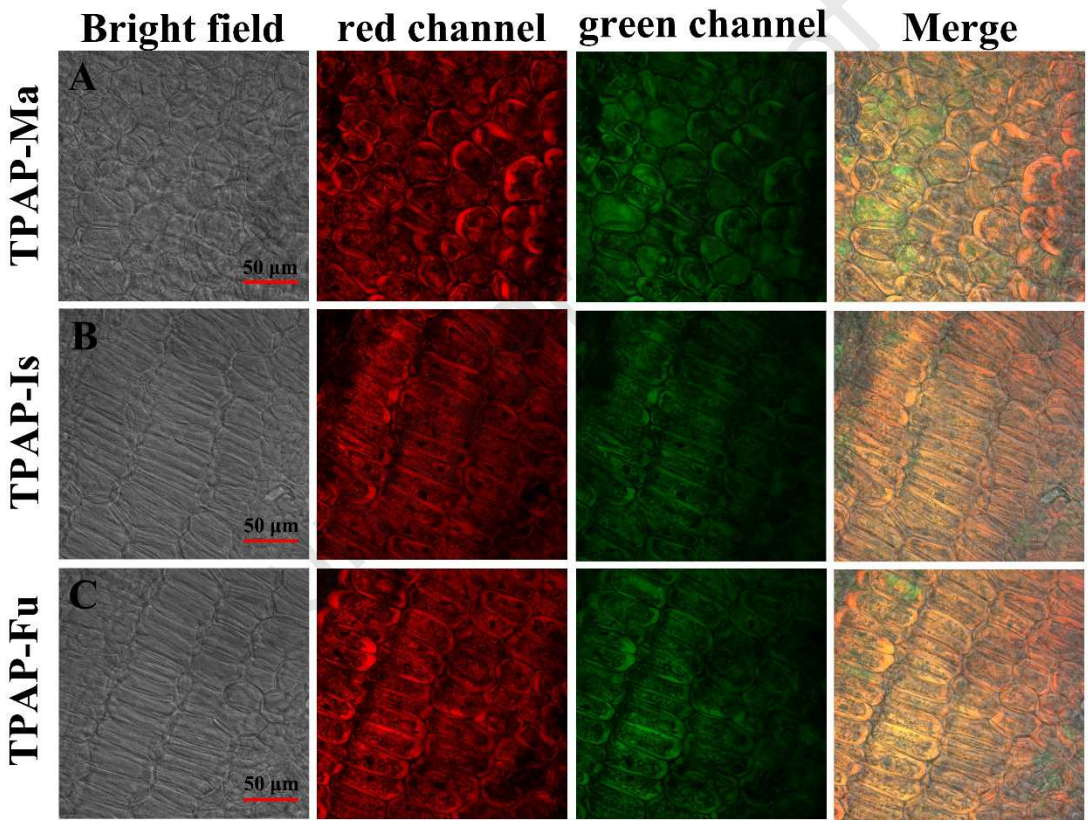

Fig. 6. Co-localization imaging of sunflower seeds stained with BODIPY 493/503 and AIEgens: (A) TPAP-Ma, (B) TPAP-Is, (C) TPAP-Fu. λex = 488 nm. Concentration: 1 μM (BODIPY 493/503 and AIEgens). Scale bar: 50 μm.

Sunflower seeds are an oil-rich plant with ample fat content and widely used as a source of oils for food. Sunflower seeds may be an ideal bioimaging material for detecting ability of probes to target LDs, although they had rarely been used in previous studies. The outer shell and the soft skin surrounding the fresh seeds were

removed, and a razor blade was used to cut transparent slices as thinly as possible. Subsequently, the seeds were incubated with BODIPY 493/503 Green (1 μM) and the three AIEgens (1 μM) for 15 min at 37 °C. Afterward, the dyes that co-marked sunflower seeds were washed three times with PBS buffer for tissue imaging experiments. As shown in Fig. 6, the probes appeared as bright-red fluorescence under the confocal laser microscope and had a good coincidence with the commercial LDs green dye, indicating that the probes can achieve rapid and highly visible LDs imaging in sunflower seeds. The results showed that these simple synthetic AIE-based probes can achieve high throughput and visualization selectivity for LDs imaging in sunflower seeds. Moreover, the results provide a new, simple, convenient, and feasible method for screening high-fat oil crops.

3.7. Photodynamic therapy

Except for LDs target in cells and tissues, these AIE molecules was expected to generate ROS for PDT under white light irradiation due to their strong push-pull structure and absorption in visible region. In this experimental section, DCF-DA was used to detect generation of ROS under light conditions. Fluorescence spectrum peak at about 525 nm enhanced when DCF-DA was oxidized to DCF by ROS. As illustrated in Fig. 7A, with the increasing time of white light irradiation (30 mW/cm^2) on TPAP-Ma, TPAP-Is, and TPAP-Fu , the fluorescence intensity of DCF-DA in the PBS solution increased rapidly up to 39-, 47-, and 53-fold in 285, 195, and 310 s, respectively. As a control, the fluorescence intensity of DCF-DA and AIEgens alone was almost constant under the same conditions. These results prompted us to explore the utilization of these AIEgen for cancer therapy quantitatively through PDT. Standard MTT assay was performed to quantitatively evaluate the killing ability of AIEgens on the model cell SMMC-7721 quantitatively under white light exposure (Fig. 7B, 7C, and 7D). Upon incubation of SMMC-7721 cells with AIEgens (up to 6.25 μM) in dark for 24 h, all AIEgens did not exhibit evident toxicity. Under light exposure for 30 min, the rate of cell apoptosis arised quickly. Only 10%-13.6% of the

cells remained viable even if the concentration of the AIEgens reached 6.25 μM. These results demonstrated the effective ROS production capacity of the AIEgens under light irradiation. Owing to the fluidity and multiple biofunctions of LDs, the ROS that are produced by these compounds with specific-targeting feature toward LDs can availably initiate to cell apoptosis, which make such probes ideal candidates for photodynamic killing of cancer cells in therapeutic applications [25].

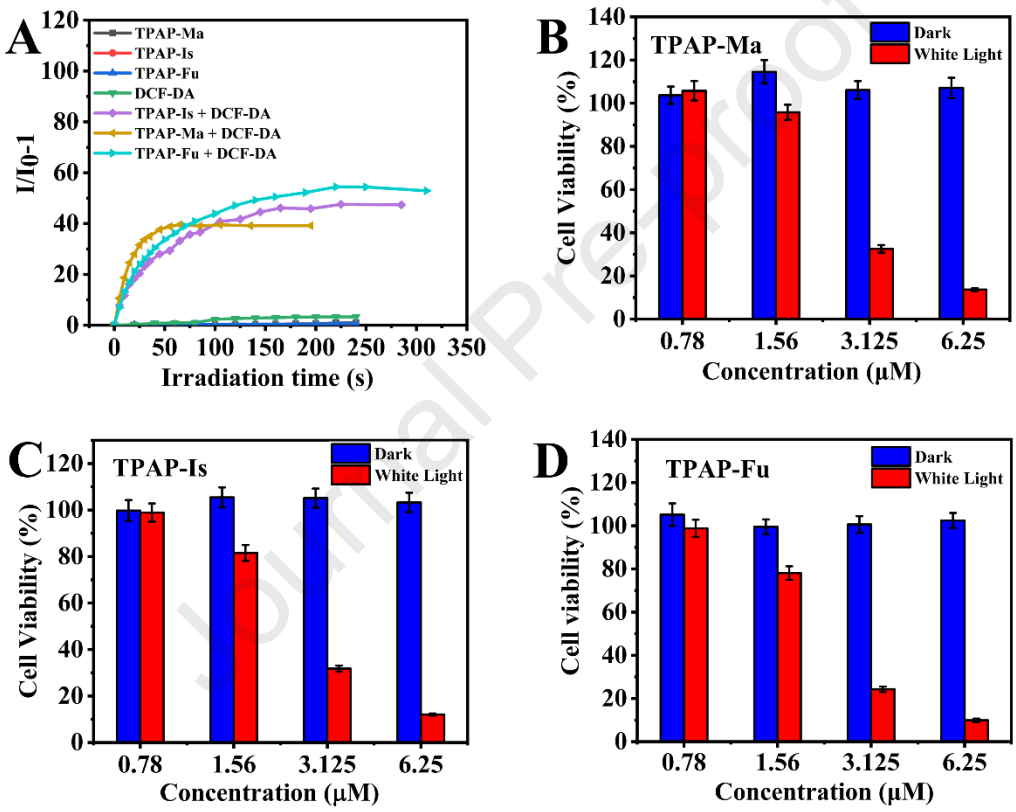

Fig. 7. ROS generation upon white light irradiation and PDT study of representative TPAP-Is. (A) Change in relative fluorescence intensity at 525 nm arisen from oxidation of DCF-DA under white light irradiation (30 mW/cm^2) with time in the absence or presence of AIEgens in PBS buffer solution. (B) Cell viability of SMMC-7721 cells stained with different concentrations of TPAP-Ma. (C) TPAP-Is and (D) TPAP-Fu under dark or in the presence of white light irradiation.

At the same time, the surprising results stimulate us to explore the killing

mechanism of ROS generated by AIEgens to cancer cell. To achieve the purpose, TPAP-Is in tricaprylin solvent (oil phase) and ROS indicator DCF-DA in PBS solution (water phase) were mixed as shown in Fig. 8A , the oil and water phase had a clear interface before light irradiation. With the irradiation time increasing, the water phase gradually turns yellow in color, which indicated the DCF-DA was oxidized by ROS. These phenomenon result in a significant increase in the fluorescence intensity of DCF-DA at 525 nm in PBS solution (Fig. 8B). To test whether the oxidation of DCF-DA is caused by a small number of compounds in water phase, the following experiments were performed. First, tricaprylin (2 mL) containing 20 μM TPAP-Is thoroughly mixed with PBS (2 mL) with a vortex mixer. Then the mixture was centrifuged and the content of TPAP-Is in aqueous phase was determined by fluorescence spectrum (Fig S20A). It is clear that the concentration of TPA-Is in the aqueous phase was more than 30 times lower than in the oil phase, despite the strong intervention of external forces. Therefore, we speculated that the ROS was mainly generated from oil phase. The ROS may be transferred to the water phase from oil-water interface. In addition, small amounts of TPAP-Is possibly enter into the water phase directly, which also result in the generation of trace ROS, and there exists a dynamic balance between the oil and water phase. The ROS in oil phase can destroy the biofunctions of LDs, the trace ROS in water phase can induce other cytoplasmic organelle damage. As a result, LDs targeted AIEgens can kill cells efficiently by PDT.

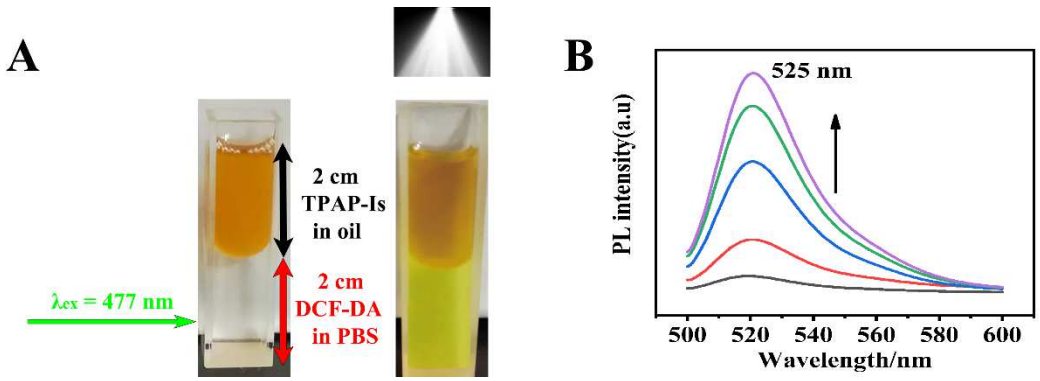

Fig. 8. (A) The sketch of spectral simulation experiment. (B) The change of fluorescence intensity at 525 nm arisen from the oxidation of DCF-DA in PBS

solution with time under light irradiation.

4. Conclusions

In summary, a series of novel AIEgens based on TPA-pyridine building block was simply synthesized with high yields. All probes can be used not only for specific targeting of LDs in cell imaging but also for LDs imaging of zebrafish and sunflower seed tissues due to their high luminance, good lipid solubility, and red NIR emission AIE characteristics. In addition, the strong D-D-π-A structure and small band gap of the probes further promote the efficient generation of ROS under white light irradiation, providing a promising choice for photodynamic therapy agents. To our knowledge, an NIR AIE fluorescent probe with high brightness and high stability and pyridine ring bridged push–pull structure has rarely been reported. This work provides an easy and practical method for constructing novel AIE fluorescent molecules for clinical research and applications in the field of photodynamic therapy.

Acknowledgements

We are thankful to the financial support from the Application and Fundamental Research Project of Shanxi Province (201801D121270, 201801D121236) and National Natural Science Foundation of PR China (No. 21571117, 21575083).

Conflict of interest There are no conflicts to declare.

References

[1] Bartz R, Li WH, Venables B, Zehmer JK, Roth MR, Welti R, et al. Lipidomics reveals that adiposomes store ether lipids and mediate phospholipid traffic. J Lipid Res 2007;48(4):837-47.

[2] Walther TC, Farese RV. The life of lipid droplets. Biochim Biophys Acta 2009;1791(6):459-66.

[3] Martin S, Parton RG. Lipid droplets: a unified view of a dynamic organelle. Nat

Rev Mol Cell Biol 2006;7(5):373-8.

[4] Olofsson SO, Bostrom P, Andersson L, Rutberg M, Perman J, Boren J. Lipid droplets as dynamic organelles connecting storage and efflux of lipids. Biochim Biophys Acta 2009;1791(6):448-58.

[5] Samuel VT, Shulman GI. Integrating mechanisms for insulin resistance: common threads and missing links. Cell 2012;148(5):852-71.

[6] Beckman M. Great balls of fat. Science 2006;311(5765):1232-34.

[7] DeBerardinis RJ, Thompson CB. Cellular metabolism and disease: what do metabolic outliers teach us?. Cell 2012;148(6):1132-44.

[8] Bozza PT, Viola JPB. Lipid droplets in inflammation and cancer. Prostaglandins Leukot Essent Fatty Acids 2010;82(4-6):243-50.

[9] Pan XY, Wilson M, McConville C, Arvanitis TN, Kauppinen RA, Peet AC. The size of cytoplasmic lipid droplets varies between tumour cell lines of the nervous system: a ^{1}H NMR spectroscopy study. Magn Reson Mater Phy 2012;25(6):479-85.

[10] Zhang C, Li JJ, Lan L, Cheng JX. Quantification of lipid metabolism in living cells through the dynamics of lipid droplets measured by stimulated raman scattering imaging. Anal Chem 2017;89(8):4502-7.

[11] Li DF, Zhao YG, Li D, Zhao HY, Huang J, Miao GY, et al. The ER-localized protein DFCP1 modulates ER-lipid droplet contact formation. Cell Rep 2019;27(2):343-58.

[12] Escobedo JO, Rusin O, Lim S, Strongin RM. NIR dyes for bioimaging applications. Curr Opin Chem Biol 2010;14(1):64-70.

[13] Yang YM, Zhao Q, Feng W, Li FY. Luminescent chemodosimeters for bioimaging. Chem Rev 2013;113(1):192-270.

[14] Qiu B, Simon MC. BODIPY 493/503 staining of neutral lipid droplets for microscopy and quantification by flow cytometry. Bio Protoc 2016;6(17):1-6.

[15] Greenspan P, Mayer EP, Fowler SD, Nile red: a selective fluorescent stain for intracellular lipid droplets. J Cell Biol 1985;100(3):965-73.

[16] Spandl J, White DJ, Peychl J, Thiele C. Live cell multicolor imaging of lipid

droplets with a new dye, LD540. Traffic 2009;10(11):1579-84.

[17] Ohsaki Y, Shinohara Y, Suzuki M, Fujimoto T. A pitfall in using BODIPY dyes to label lipid droplets for fluorescence microscopy. Histochem Cell Biol 2010;133(4):477-80.

[18] Luo JD, Xie ZL, Lam JWY, Cheng L, Chen HY, Qiu CF, et al. Aggregation-induced emission of 1-methyl-1,2,3,4,5-pentaphenylsilole. Chem Commun 2001(18):1740-1.

[19] Zhu CL, Kwok RTK, Lam JWY, Tang BZ. Aggregation-induced emission: a trailblazing journey to the field of biomedicine. ACS Applied Bio Materials 2018;1(6):1768-86.

[20] Yuan YY, Feng GX, Qin W, Tang BZ, Liu B. Targeted and image-guided photodynamic cancer therapy based on organic nanoparticles with aggregation-induced emission characteristics. Chem Commun 2014;50(63):8757-60.

[21] Hilderbrand SA, Weissleder R. Near-infrared fluorescence: application to in vivo molecular imaging. Curr Opin Chem Biol 2010;14(1):71-9.

[22] Yuan L, Lin WY, Zheng KB, He LW, Huang WM. Far-red to near infrared analyte-responsive fluorescent probes based on organic fluorophore platforms for fluorescence imaging. Chem Soc Rev 2013;42(2):622-61.

[23] Roncali J. Synthetic principles for bandgap control in linear π-conjugated systems. Chem Rev 1997;97(1):173-205.

[24] Zhang FL, Di YZ, Li Y, Qi QK, Qian JY, Fu XQ, et al. Highly efficient far red/near-Infrared fluorophores with aggregation-induced emission for bioimaging. Dyes Pigments 2017;142:491-8.

[25] Wang D, Su HF, Kwok RTK, Shan GG, Leung ACS, Lee MMS, et al. Facile synthesis of red/NIR AIE luminogens with simple structures, bright emissions, and high photostabilities, and their applications for specific imaging of lipid droplets and image-guided photodynamic therapy. Advanced Functional Materials 2017;27(46):1704039.

[26] Zheng Z, Zhang TF, Liu HX, Chen YC, Kwok RTK, Ma C, et al. Bright near-infrared aggregation-induced emission luminogens with strong two-photon

absorption, excellent organelle specificity, and efficient photodynamic therapy potential. ACS Nano 2018;12(8):8145-59.

[27] Xu SD, Yuan YY, Cai XL, Zhang CJ, Hu F, Liang J, et al. Tuning the singlet-triplet energy gap: a unique approach to efficient photosensitizers with aggregation-induced emission (AIE) characteristics. Chem Sci 2015;6(10):5824-30.

[28] Wu WB, Mao D, Hu F, Xu SD, Chen C, Zhang CJ, et al. A highly efficient and photostable photosensitizer with near-infrared aggregation-induced emission for image-guided photodynamic anticancer therapy. Adv Mater. 2017;29(33):1700548.

[29] Chou HH, Hsu CY, Hsu YC, Lin YS, Lin JT, Tsai C. Dipolar organic pyridyl dyes for dye-sensitized solar cell applications. Tetrahedron 2012;68(2):767-73.

[30] Kaur P, Kaur M, Singh K. Ferrocene based chemosensor for Cu^{2+}-a dual channel signaling system. Talanta 2011;85(2):1050-5.

[31] Hou JT, Ko KP, Shi H, Ren WX, Verwilst P, Koo S, et al. PLK1-targeted fluorescent tumor imaging with high signal-background-ratio. ACS Sens 2017;2(10):1512-6.

[32] Mathivanan M, Tharmalingam B, Lin CH, Pandiyan BV, Thiagarajan V, Murugesapandian B. ESIPT-active multi-color aggregation-induced emission features of triphenylamine-salicylaldehyde-based unsymmetrical azine family. CrystEngComm 2020;22(2):213-28.

[33] Grabowski ZR, Rotkiewicz K, Rettig W. Structural changes accompanying intramolecular electron transfer: focus on twisted intramolecular charge-transfer states and structures. Chem Rev 2003;103(10):3899-4032.

[34] Gu XG, Zhao EG, Lam JWY, Peng Q, Xie YJ, Zhang YL, et al. Mitochondrion-specific live-cell bioprobe operated in a fluorescence turn-on manner and a well-designed photoactivatable mechanism. Adv Mater 2015;27(44):7093-100.

[35] Gibson J, Monkman AP, Penfold TJ. The importance of vibronic coupling for efficient reverse intersystem crossing in thermally activated delayed fluorescence molecules. ChemPhysChem 2016;17(19):2956-61.

[36] Hu F, Xu SD, Liu B. Photosensitizers with aggregation-induced emission: materials and biomedical applications. Adv Mater 2018;30(45):1801350.

[37] Lu HG, Zheng YD, Zhao XW, Wang LJ, Ma SQ, Han XQ, et al. Highly efficient far red/near-infrared solid fluorophores: aggregation-induced emission, intramolecular charge transfer, twisted molecular conformation, and bioimaging applications. Angew Chem Int Ed 2016;55(1):155-9.

[38] Horobin RW, Rashid-Doubell F. Predicting small molecule fluorescent probe localization in living cells using QSAR modeling.2. specifying probe, protocol and cell factors; selecting QSAR models; predicting entry and localization. Biotech Histochem 2013;88(8):461-76.

[39] Witherel CE, Gurevich D, Collin JD, Martin P, Spiller KL. Host-biomaterial interactions in zebrafish. ACS Biomater Sci Eng 2017;4(4):1233-40.

Highlights

Three novel near-infrared AIE-based fluorophores were synthesized.

These AIEgens can highly light up LDs in cells, zebrafish and sunflower seed.

They can be applied in PDT through targeting LDs.

The authors declare no conflicts of interest.